Precision measurement of the nuclear polarization in laser-cooled, optically pumped ^{37}K

2016 New J. Phys. 18 073028

(http://iopscience.iop.org/1367-2630/18/7/073028)

New Journal of Physics
The open access journal at the forefront of physics

Deutsche Physikalische Gesellschaft DPG
IOP Institute of Physics

Published in partnership with: Deutsche Physikalische Gesellschaft and the Institute of Physics

OPEN ACCESS

RECEIVED
9 February 2016

REVISED
30 May 2016

ACCEPTED FOR PUBLICATION
23 June 2016

PUBLISHED
13 July 2016

PAPER

Precision measurement of the nuclear polarization in laser-cooled, optically pumped ^{37}K

B Fenker[1,2,7], J A Behr[3], D Melconian[1,2,7], R M A Anderson[3], M Anholm[3,4], D Ashery[5], R S Behling[1,6], I Cohen[5], I Craiciu[3], J M Donohue[3], C Farfan[3], D Friesen[3], A Gorelov[3], J McNeil[3], M Mehlman[1,2], H Norton[3], K Olchanski[3], S Smale[3], O Thériault[3], A N Vantyghem[3] and C L Warner[3]

[1] Cyclotron Institute, Texas A&M University, 3366 TAMU, College Station, TX 77843-3366, USA
[2] Department of Physics and Astronomy, Texas A&M University, 4242 TAMU, College Station, TX 77842-4242, USA
[3] TRIUMF, 4004 Wesbrook Mall, Vancouver, BC V6T 2A3, Canada
[4] Department of Physics and Astronomy, University of Manitoba, Winnipeg, MB R3T 2N2, Canada
[5] School of Physics and Astronomy, Tel Aviv University, Tel Aviv, Israel
[6] Department of Chemistry, Texas A&M University, 3012 TAMU, College Station, TX 77842-3012, USA
[7] Authors to whom any correspondence should be addressed.

E-mail: ben@fenker.org **and** dmelconian@comp.tamu.edu

Keywords: Beta-decay, fundamental symmetries, optical pumping, atom trapping, parity violation

Abstract

We report a measurement of the nuclear polarization of laser-cooled, optically pumped ^{37}K atoms which will allow us to precisely measure angular correlation parameters in the β^+-decay of the same atoms. These results will be used to test the $V - A$ framework of the weak interaction at high precision. At the TRIUMF neutral atom trap (TRINAT), a magneto-optical trap confines and cools neutral ^{37}K atoms and optical pumping spin-polarizes them. We monitor the nuclear polarization of the same atoms that are decaying *in situ* by photoionizing a small fraction of the partially polarized atoms and then use the standard optical Bloch equations to model their population distribution. We obtain an average nuclear polarization of $\bar{P} = 0.9913 \pm 0.0009$, which is significantly more precise than previous measurements with this technique. Since our current measurement of the β-asymmetry has 0.2% statistical uncertainty, the polarization measurement reported here will not limit its overall uncertainty. This result also demonstrates the capability to measure the polarization to $<0.1\%$, allowing for a measurement of angular correlation parameters to this level of precision, which would be competitive in searches for new physics.

1. Introduction

Measurements in nuclear β-decay have historically contributed to the establishment of the standard model of electroweak physics as a theory containing massive bosons coupling only to left-handed chirality leptons. Today, precision measurements search for and constrain possible new physics. For example, in isobaric analog, mixed Fermi–Gamow Teller $\beta^{\pm}$ decays, the angular distribution of the leptons with respect to the spin direction of the parent nucleus is sensitive to a variety of new physics including right-handed currents and scalar or tensor interactions [1–4]. Additionally, if we ignore this class of standard model extensions, this measurement can be combined with other measurements of isospin $T = 1/2$ mirror-transitions to extract the V_{ud} element of the Cabibbo–Kobayashi–Maskawa quark mixing matrix [5, 6]. This technique is complementary to and independent of the most precise value obtained using $T = 0$ super-allowed decays [7]. In general, to complement high-energy searches for exotic currents in the weak interaction, these experiments should aim for a precision of $\sim 0.1\%$ [8].

To reach this ambitious goal, we have developed the techniques at the TRIUMF neutral atom trap (TRINAT) to confine the β^+-emitter, ^{37}K ($I^{\pi} = 3/2^+ \rightarrow 3/2^+$, $t_{1/2} = 1.2$ s), in an alternating current magneto-optical trap

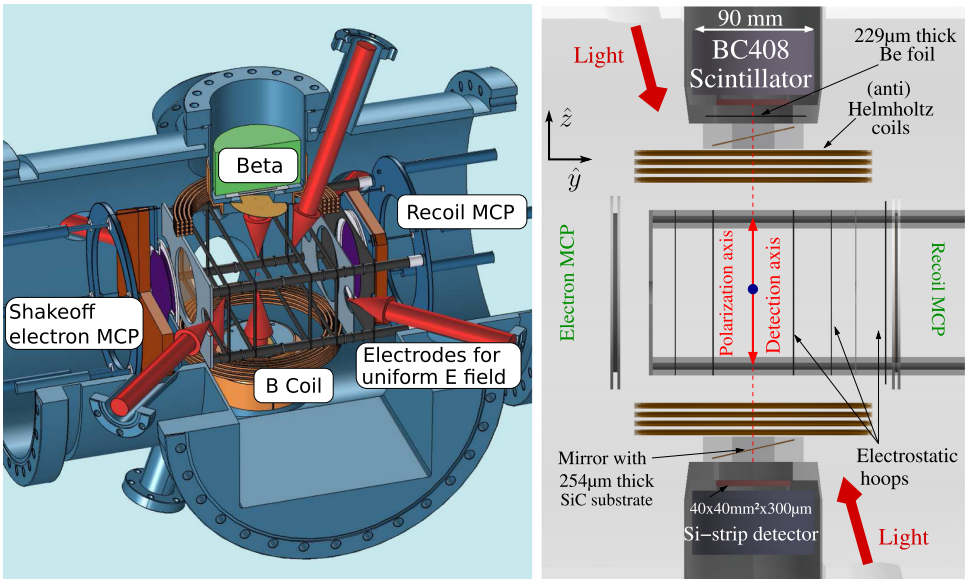

Figure 1. The main TRINAT detection chamber. The red arrows on either panel indicate the direction of incoming light for both the MOT and OP lasers. To polarize the atoms along the axis defined by scintillator and silicon strip detectors, which are opaque, the light is brought in at a 9.5° angle with respect to normal incidence and reflected off of a thin mirror. These detectors are placed symmetrically along the vertical axis and are housed in a re-entrant flange which is separated from the vacuum by a thin Be foil. Also visible are the water-cooled magnetic field coils which provide the Helmholtz (OP) and anti-Helmholtz (MOT) fields as well as the electrostatic hoops that generate a nearly uniform electric field. The recoil microchannel plate detector (MCP) is at negative electric potential, while the electron MCP is at positive potential.

(AC-MOT) [9, 10] and observe its decay products [11, 12]. Furthermore, the atoms are spin-polarized by optical pumping (OP) while the MOT is off, creating an ideal source of polarized atoms decaying nearly from rest in an exceptionally open geometry.

Using this setup, we have previously measured the ν-asymmetry (B_ν in [13]) to 3.6% uncertainty [11] and the β-asymmetry (A_β) to 1.5% uncertainty [14]. Although the polarization measurement in [14] was consistent with tests using naturally occurring ^{41}K, the *in situ* measurement of ^{37}K polarization was limited by statistics. We have recently taken data for a second measurement of A_β with the goal of a final uncertainty less than 0.5%; more precise than any previous measurement in a nucleus. Once reaching this level of precision, we will evaluate the prospects for an even-more-precise measurement.

In our geometry shown in figure 1, the β-asymmetry can be simply determined using:

$$A_\beta = \frac{A_{\rm obs}}{P} = \frac{1}{P}\frac{r^\uparrow - r^\downarrow}{r^\uparrow + r^\downarrow}. \tag{1}$$

Here, $A_{\rm obs}$ is the observed β-asymmetry as measured in the nuclear detectors, P is the nuclear polarization, and $r^\uparrow$ ($r^\downarrow$) is the rate of positrons detected along (against) the nuclear polarization direction. In forming the asymmetry in equation (1), it is possible to use a symmetric pair of detectors along a fixed polarization axis or to use a single β-detector and periodically reverse the sign of the polarization. In our case, we eliminate many systematic effects by doing both, utilizing the 'super-ratio' technique [15, 16]. In addition to the nuclear measurement of $A_{\rm obs}$, a measurement of A_β requires a precision measurement of the degree of nuclear polarization, defined by:

$$\vec{P} = \frac{\langle \vec{I} \rangle}{I}. \tag{2}$$

Here, $\vec{I}$ is the nuclear polarization vector and, $I = 3/2$ is its magnitude. Furthermore, since the nuclear spin is greater than 1/2, the atoms have additional internal degrees of freedom, proportional to the next moment of the nuclear spin projection. We define the nuclear alignment term as:

$$T = \frac{I(I+1) - 3\langle(\vec{I}\cdot\hat{\imath})^2\rangle}{I(2I-1)}, \tag{3}$$

where $\hat{\imath}$ is a unit vector in the direction of $\vec{I}$. Although it does not contribute directly to the positron asymmetry (see footnote 7 in [13]), it does contribute to angular correlations involving the neutrino momentum, which can

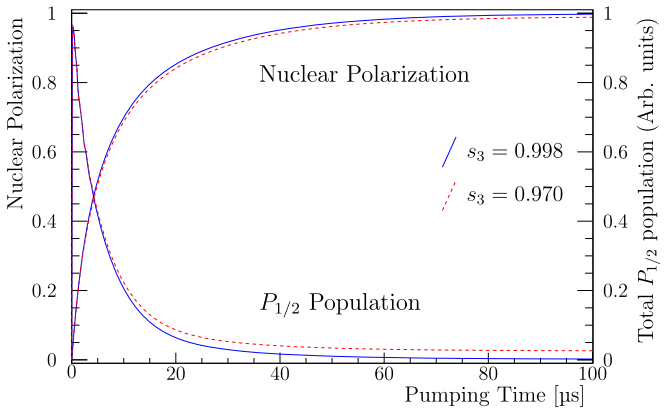

Figure 2. Simulated time evolution of optical pumping with $\sigma^{\pm}$ light on the D_1 transition. The photoionization is observed and used to infer the nuclear polarization by comparing to a numerical simulation of optical pumping. As the rate of photoionization in the region $t \to \infty$ decreases, the degree of polarization increases towards unity. The atoms are considered fully polarized after the optical pumping light has been on for 100 μs (see section 5.1). The parameter s_3 gives the degree of circular polarization and is defined in section 2.2. The nuclear alignment term follows the same measurement strategy.

be inferred from the simultaneous measurement of the momentum of the β and nuclear recoil. Therefore, we include it here for completeness.

We have collected statistics for a measurement of $A_{\rm obs}$ with statistical uncertainty $\Delta A_{\rm obs}/A_{\rm obs} = 0.2\%$ and, therefore, must measure the nuclear polarization to a similar level of precision so that the polarization measurement does not dominate the final uncertainty.

To polarize the atoms, we optically pump them, with the MOT off, on the D_1 transition with circularly polarized ($\sigma^{\pm}$) light. This accumulates atoms in the state with $m_F = \pm F$ corresponding to complete *nuclear* polarization. Here, $\vec{F} = \vec{I} + \vec{J}$ where $\vec{J}$ is the atomic angular momentum. To monitor the polarization, we photoionize a small fraction of the atoms which have been excited to the $P_{1/2}$ state by the OP light. This provides a cleaner signal with fewer trapped atoms compared to monitoring the fluorescence. The total $P_{1/2}$ population is a sensitive probe of the nuclear polarization because atoms must have been excited from a partially polarized $S_{1/2}$ state with $|m_F| < F$. Therefore, the $P_{1/2}$ population is related to the number of partially polarized or unpolarized atoms. Finally, we fit a numerical simulation of OP to the photoion time spectrum and deduce the nuclear polarization from the result. A typical simulation demonstrating the principle of the technique is shown in figure 2. In this paper, we present the results of this nuclear polarization measurement, which is significantly more precise than previous results with this method [11, 14].

2. Experimental methods

Nuclear β-decay and atom-trap experimental methods used by TRINAT are described in [17]. Here, we will describe the apparatus with a particular emphasis on the polarization measurement. First, we give a description of the entire apparatus in section 2.1. Following this, sections 2.2 and 2.3 describe the two depolarizing mechanisms that lead to $|P| < 1$, and section 2.4 describes the UV light used to monitor the nuclear polarization.

2.1. General description

Ions of the short-lived isotope ^{37}K are delivered from ISAC, the radioactive beam facility at TRIUMF, and neutralized on a hot zirconium foil [18]. The atoms are then collected in a vapor-cell MOT in a preparation chamber with 0.1% efficiency [19]. To suppress a background from untrapped atoms, they are then transferred with 75% efficiency by a red-detuned pulsed laser 'push-beam' to a second MOT where the precision measurement takes place [20]. The push beam is controlled by a double-pass acousto-optic modulator (AOM) setup, is turned on only briefly during atom transfers, and misses the second trap by aiming the beam 1 cm above the measurement trap's height except during atom transfers.

Since the MOT destroys any polarization, it must be turned off and on rapidly so that there is sufficient time to optically pump the atoms and collect polarized decay data while the previously confined atoms expand ballistically. The confining forces are then turned back on to re-collect the atoms before the cloud's expansion causes a significant loss of atoms from the trapping region. The trapping beam itself is switched off to less than 10^{-4} of its maximum value by turning off the first-order diffracted beam from an AOM. Any remaining trap

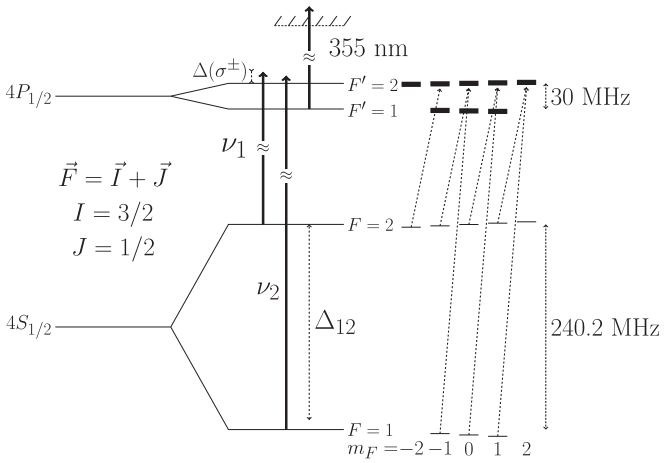

Figure 3. The fine and hyperfine structure of ^{37}K showing the laser transitions relevant to optical pumping. The natural linewidth of the $4P_{1/2}$ state is 6 MHz. Circularly polarized light brought in along the vertical axis (see figure 1) and tuned to the D_1 transition pumps atoms into the $F = 2$, $m_F = \pm 2$ state, resulting in a very high cloud polarization. The parameter Δ gives the detuning from the $F = 2 \rightarrow F' = 2$ resonance and is different for the σ^+/σ^- polarization states. The second frequency is detuned a fixed amount, Δ_{12}, from this frequency and optically pumps atoms which occupy $F = 1$ ground states. Neither Δ nor Δ_{12} are shown to scale. The 355 nm light continually probes the excited state population by photoionizing atoms from the excited P states, which are subsequently detected by the recoil MCP.

light is from the tail of the zeroth-order beam, 90 MHz (15 linewidths) off-resonance. The resulting excitation is less than 2×10^{-4} of the OP light.

In order to rapidly eliminate the magnetic field used for trapping, an AC-MOT is used [9, 10]. In this scheme, an AC current is run through the anti-Helmholtz coils (see figure 1) instead of the usual DC current. The resultant magnetic field produced by the coils varies sinusoidally in time, as does the field that results from induced eddy currents in nearby materials, though the two components differ in phase. Then, in order to minimize the residual magnetic field after shutting off the MOT, the current through the coils is shut off when the combined magnetic field is zero. The optimal shutoff phase is a function of chamber geometry and material, as well as the frequency of the AC current [9].

In order to trap atoms in a sinusoidally varying magnetic field, it is necessary to vary the polarization of the MOT's trapping beam as well. This is achieved by the use of an electro-optic modulator, set to adjust the trapping beam between two polarization states in phase with the magnetic field, such that a confining force is produced at all times.

Once the AC-MOT is off, the ballistically expanding atoms are optically pumped with circularly polarized light on the D_1 ($4S_{1/2} \rightarrow 4P_{1/2}$) transition (see figure 3). Note that the atoms must be polarized along the axis connecting a pair of opaque detectors as shown in figure 1. In order to allow the light to propagate in this direction, the light is brought in at a 19° angle with respect to the polarization axis and reflected off of a thin SiC mirror before interacting with the atoms.

Furthermore, a static magnetic field, $B_z = 2.3$ G, is applied along the quantization axis to break the degeneracy of the Zeeman sublevels. As a result of the OP, atoms accumulate in the $4S_{1/2}|F = 2,\ m_F = \pm 2\rangle$ (fully stretched) state depending on the sign of circular polarization. This state corresponds to complete atomic *and* nuclear polarization.

To minimize systematic effects, the polarization state is reversed every 16 s and simultaneously a frequency shift of $\Delta(\sigma^+) - \Delta(\sigma^-) = 4$ MHz (see figure 3) is applied. This is done in order to move closer to the desired $m_F = \pm 1 \rightarrow m_{F'} = \pm 2$ transition frequency while moving further from the unwanted $m_F = \pm 2 \rightarrow m_{F'} = \pm 1$ transition, which can be excited by a component of the OP light circularly polarized with the 'wrong' sign. Note that the sign of B_z is not changed throughout the experiment.

The nuclear polarization is measured by monitoring the total $P_{1/2}$ population of the atoms. Atoms that have been fully polarized are not excited by the OP light and, therefore, remain in a fully stretched $S_{1/2}$ ground state until the MOT light is switched back on. As shown in figure 2, observing a decrease in the $P_{1/2}$ population implies an increase in $|P|$.

The $P_{1/2}$ population could be monitored by detecting the fluorescence light as atoms de-excite to an $S_{1/2}$ state. However, the collection efficiency of the first MOT as well as the flux of ^{37}K delivered by ISAC limit the experiment to $\sim 10^4$ atoms at a time. With this number of atoms, the time-resolved fluorescence signal has a poor signal-to-noise ratio S/N and does not provide a clean signal.

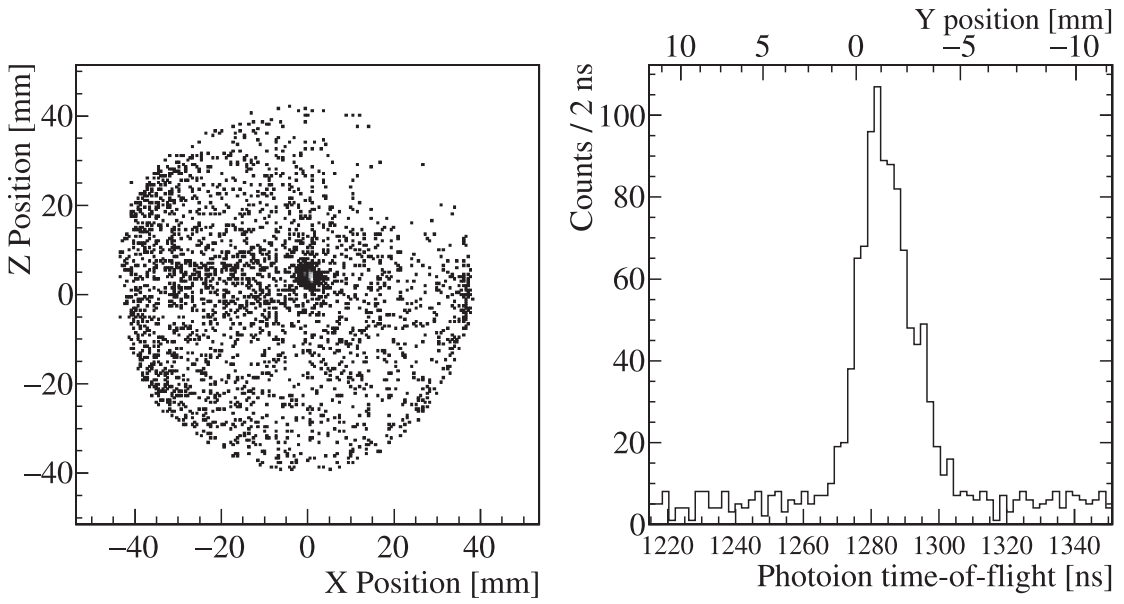

Figure 4. Photoion position and time-of-flight spectrum demonstrating the clean signal. The left panel shows events gated on the central time-of-flight peak while the right panel shows events requiring that the position is in the dense region at the center of the plate. The region of the plate nearly devoid of events has lower detection efficiency, but it does not affect the polarization measurement.

For this reason, we photoionize a small fraction of the atoms in the $P_{1/2}$ state using UV light at 355 nm and pulsed at a 10 kHz repetition rate. The UV photons do not have the energy necessary to photoionize atoms in the $S_{1/2}$ ground state so that photoions are generated only from atoms that have been excited to the $P_{1/2}$ state by the OP laser.

A uniform electric field generated by the series of electrostatic hoops shown in figure 1 sweeps the photoions onto the microchannel plate (MCP) detector at negative electric potential where they are observed in coincidence with the UV light. The MCP detector is backed by a delay-line anode for position sensitivity. As a result, the photoion spectrum shown in figure 4 is clean: the photoions are well resolved both spatially and in time-of-flight.

However, the photoionization rate has no sensitivity to the distribution of the partially polarized atoms throughout the Zeeman sublevels with $|m_F| < F$. Although this population can be made quite small, the precision measurement described here requires knowledge of its distribution. There have been methods developed to probe this directly [21–23], but the specific constraints of our experiment, including the relatively low number of trapped atoms, make these impractical. Additionally, the polarization measurement must be non-destructive, preserving the polarization of the atoms in order to observe the β-asymmetry in the nuclear decay of the same atoms.

To satisfy these requirements, we adopt the method of monitoring the $P_{1/2}$ population with photoionization as described above and modeling the sublevel distribution of the partially polarized atoms as presented in section 3. We emphasize that the $P_{1/2}$ population, inferred from the photoionization measurement, is directly proportional to the total partially polarized population, and the theoretical model must only determine the sublevel distribution of this relatively small population.

In addition to the polarization described above, a measurement of A_β requires a simultaneous determination of the β-asymmetry, $A_{\rm obs}$. The β-asymmetry is measured by a pair of β-telescopes placed along the vertical polarization axis. Although this arrangement requires an extra reflection of the OP light, it allows the measurement of $A_{\rm obs}$ to have the highest sensitivity. Each β-telescope consists of a thin Si-strip detector backed by a thick plastic scintillator. The scintillator fully stops the positrons from the ^{37}K decay ($Q_{\rm EC} = 6.1{\rm MeV}/c^2$) and records their full energy. The Si-strip detector provides position information and, due to its low efficiency for detecting γ-rays, suppresses the background from 511 keV annihilation radiation. To identify decays that occurred within the region of OP, we detect low energy shake-off e^- which accompany β^+ decay by sweeping them with an electric field towards a MCP detector and observing them in coincidence with the β^+. This combination of detectors provides an exceptionally clean signal, almost entirely free from backgrounds.

Having described the apparatus generally, we now give a detailed description of the elements necessary to produce highly polarized nuclei and measure the degree of polarization.

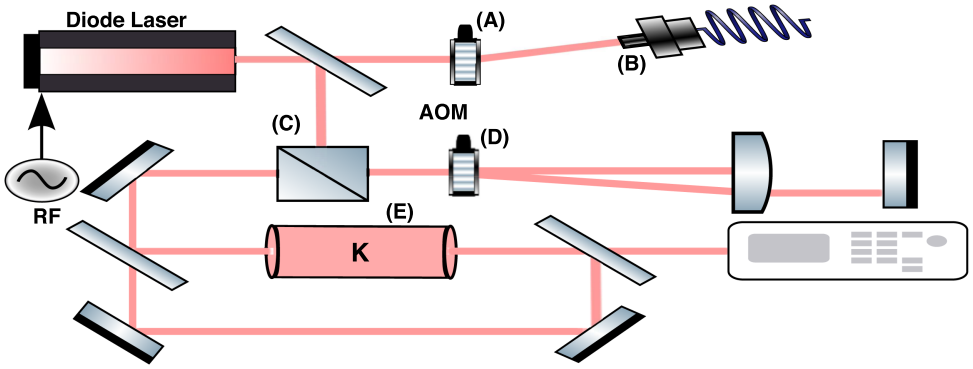

Figure 5. Optical pumping light and frequency locking scheme to maintain constant light profile with different isotopes. The $F = 2 \rightarrow F' = 2$ and $F = 1 \rightarrow F' = 1$ frequencies are generated by RF modulation of the diode laser current. The OP light is turned on and off by changing the RF input frequency of an AOM (A), whose first-order diffraction is steered on and off an optical fiber (B). That scheme, unlike turning the RF power on and off, keeps the AOM at near-constant temperature, avoiding steering and light profile distortion as the light is injected into the optical fiber; thus the light power is switched well from zero to full value without transients. 10% of the light is diverted to lock the laser frequency (C). The light is shifted in frequency by a tunable double-pass AOM (D) before going to a vapor cell of potassium (E), allowing frequency locking either for naturally occurring ^{41}K, or for accelerator-produced ^{37}K, by referencing to Doppler-free Zeeman-dithered saturation absorption peaks of stable isotopes [26].

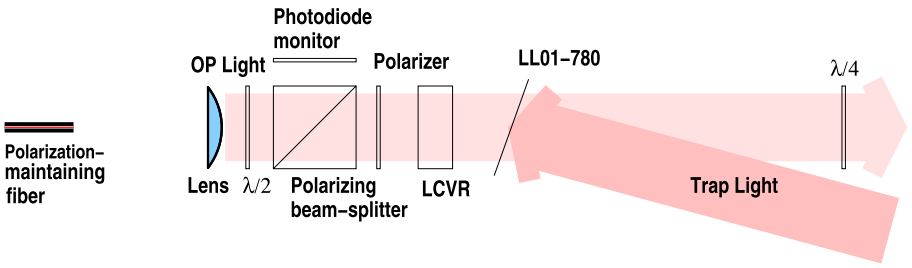

Figure 6. Optical elements creating the circularly polarized D_1 light. This arrangement is repeated for both OP arms The liquid crystal variable retarder (LCVR) is used to control the sign of the circular polarization of the OP light and the LL01-780 laser line filter is used to combine the OP and MOT light along the same optical path.

2.2. OP light

To obtain the highest polarization, both the $F = 1$ and $F = 2$ ground states must be optically pumped. The two frequencies needed to accomplish this are created by RF power injected directly into the diode laser with the frequency close to the ground state hyperfine splitting. We apply this standard technique [24] at relatively low RF power levels that produce light at about 1/2 the power of the carrier frequency and split from the carrier frequency by the RF frequency. This frequency is easily adjusted from the hyperfine splitting of ^{41}K (254 MHz) to ^{37}K (240 MHz) without changing the alignment or beam spatial quality. The optical sideband strength is monitored with a Fabry–Perot cavity and is stable in power to about 10%.

The saturation spectroscopy and double-pass AOM setup shown in figure 5 allows frequency locking for either ^{41}K or ^{37}K. The light is also detuned 1 MHz with respect to the ground-state hyperfine splitting to completely destroy dark state coherences [25] (see section 4). Following this, the light is divided into two beams and injected into polarization-maintaining optical fibers. The remainder of the optical path after exiting these optical fibers is shown in figure 6.

After exiting the optical fiber, the OP light passes through a polarizing beam-splitter and contrast 5×10^4, 25 mm diameter suspended silver nanoparticle linear polarizer (CODIXX ColorPol VIS 700 BC4). This is shown in figure 6. Next, the polarization state is determined by the voltage applied to a liquid crystal variable retarder which either maintains the linear polarization or rotates it 90°.

Since the OP and MOT light must travel the same path through the vacuum chamber, they are combined by an angle-tuned laser line filter. This Semrock LL01-780 nominally transmits 98% of 766.49 nm OP light while reflecting 98% of the 769.9 nm MOT light at 20° incidence. The transmission of OP light changes by 4% between the linear polarization states. The output of this feeds a high-quality 1/4-wave plate before being injected into the vacuum chamber. Note that there are no lenses in the path after the polarizer, avoiding position-dependent birefringence.

Table 1. Results of the measurement of the OP light polarization. The direct measurement of s_3^{in} is done before the viewport, and the value after the viewport (s_3^{out}) includes a calculation of the effect of the birefringence in each viewport.

	Laser port	s_3^{in}	s_3^{out}
σ^-	Upper	−0.9980(4)	−0.9958(8)
	Lower	−0.9990(10)	−0.9984(13)
σ^+	Upper	0.9931(9)	0.9893(14)
	Lower	0.9997(3)	0.9994(5)

The quality of circular polarization is critical to the final nuclear polarization achieved. Any component of the light with the 'wrong' polarization removes atoms from the fully polarized state and drives $|P| < 1$. We parametrize the quality of circular polarization with the normalized Stokes parameter:

$$s_3 = \frac{\mathcal{I}_+ - \mathcal{I}_-}{\mathcal{I}_+ + \mathcal{I}_-}, \tag{4}$$

where $\mathcal{I}_+$ ($\mathcal{I}_-$) is the laser intensity in the σ^+ (σ^-) state.

The degree of linear polarization is measured in each polarization state along both OP arms immediately before passing through the atom-trap viewports and s_3 is determined for each case. However, stress-induced birefringence in the viewport glass can change the light ellipticity. We characterize this birefringence by its effect on s_3 as the light passes through the viewport. If the s_3 parameter of the incoming light is denoted s_3^{in}, then this same parameter for the light after it has passed through the viewport is given by [27]:

$$s_3^{\text{out}} = \sin(\arcsin(s_3^{\text{in}}) + \Delta n\, kL), \tag{5}$$

where Δn parametrizes the effect of the viewport, k is the wave number of the light and L is the thickness of the viewport glass.

We developed viewports to minimize Δn, replacing the elastomer in a commercial viewport with PCTFE, which is compatible with UHV [27]. We obtain $\Delta n = (-6 \pm 2) \times 10^{-6}$ and $(-2 \pm 1) \times 10^{-6}$ for the two arms respectively. Although this measurement is done with the viewports in air, we have measured the cumulative effect of both viewports on s_3 both in air as well as with the viewports under vacuum and observe no difference. This is consistent with the pressure on the viewports having no effect on Δn. The measured values for s_3 both before and after the viewport are shown in table 1.

After entering the vacuum chamber, the light must be reflected once as shown in figure 1. The mirror used for this purpose is coated with a commercial dielectric stack with 99.5% reflectivity. We observe a change in the outgoing light's ellipticity $|s_3' - s_3| < 10^{-4}$ at 9.5° incidence.

The alignment of the OP light, which defines the polarization axis, is done at the two viewports; the mirror is fixed with mechanical precision. The result is that the light is aligned to $\Delta\theta = 1$ mrad with respect to the vacuum chamber and, therefore, to the detection axis. Since the β-asymmetry (see [13], equation (2)) is proportional to $\cos\theta$, this produces a negligible error of 5×10^{-7}.

2.3. Magnetic fields

A second mechanism that can drive $|P| < 1$ is a magnetic field transverse to the OP axis (B_x) that causes Larmor precession out of the stretched state. We have carefully designed the apparatus to minimize eddy currents once the AC-MOT is turned off, which in turn produce a magnetic field. Non-magnetic materials such as 316 L and 316LN grade stainless steel and titanium were used wherever possible and the chamber welds were kept thin to minimize their magnetic permeability. We measured the relative permeability of the welds to be <1.25. The vacuum chamber has a large (12 in) diameter to place potentially magnetic materials as far away from the trapped atoms as reasonably possible. The nearest material to the atoms is the set of electrostatic hoops shown in figure 1 which direct the photoions onto the MCP. These are made from SIGRADUR G grade glassy carbon, a semiconductor with resistivity 4500 $\mu\Omega$ cm, two orders of magnitude better than stainless steel.

In order to cancel out magnetic fields that are constant on the time scale of OP, we arranged two pairs of magnetic trim coils exterior to the vacuum chamber. By varying the DC current in these coils, we were able to apply a transverse magnetic field to cancel stray fields at the location of the trapped atoms.

To optimize these settings, we optically pumped ^{41}K, which can be trapped in large numbers and has a similar hyperfine structure to ^{37}K. We used the same system described in this section except that we monitored the fluorescence directly rather than the photoionization. Keeping all the laser parameters fixed, we scanned the

trim-coil current and observed the residual fluorescence after OP. The minimum residual fluorescence corresponds to the optimal current setting which was also used for the ^{37}K experiment.

Additionally, the AC quadrupole magnetic field is switched off before the OP begins but induces eddy currents in the surrounding material, which in turn produce a magnetic field. Although the purpose of using an AC-MOT is to reduce these eddy currents by turning off the magnetic field when it is nearly zero, we used a Hall probe to measure an initial residual field of 103 mG cm^{-1}, which decays to a final value of 22 mG cm^{-1} with a time constant of $\sim$130 μs. Although this measurement was done with one vacuum flange removed, it demonstrates both the approximate size of this effect as well as the need, described in section 5.1, to wait until this field has completely decayed away before starting OP.

2.4. Photoionization light

The 355 nm UV light that photoionizes the excited atoms is circularly polarized and has a near-TEM$_{00}$ mode with a $1/e^2$ diameter of 12 mm. It comes from a commercial diode-pumped solid-state pulsed laser making 0.5 ns pulses at 10 kHz repetition rate. The light propagates at 35° with respect to the OP axis. After interacting with the atoms, the UV light is reflected along the same path in order to provide a second opportunity to interact with the atoms with $\sim$90% of the original intensity. Next the sign of the polarization is reversed, and the light again interacts with the atoms twice, although with the third pass now at 41% of the original intensity. In total, the UV light photoionizes about $1/10^6$ atoms per pulse. The effects of the UV light polarization on the photoionization signal are discussed in section 3.

Note that the cross-section of photoionization is on the order of 1 Mb, while Rayleigh scattering has a cross-section 10^6 lower. Therefore, the 355 nm light is effectively a passive probe that does not disturb the system. It either photoionizes the atom, removing it from the population so its subsequent less-polarized β-decay is not observed, or has negligible probability of disturbing the polarization.

3. Theoretical model

Having described the experimental setup, we now describe the model used to calculate the sublevel distribution of the small fraction of atoms that are *not* fully polarized. Although this population is small, at the current level of precision, its distribution can impact the nuclear polarization achieved.

Our theoretical OP calculation is based on a semi-classical approach using the density operator formalism, i.e., the standard optical Bloch equations with the phenomenological spontaneous decay term $R(t)$

$$\frac{\mathrm{d}\rho(t)}{\mathrm{d}t} = \frac{1}{\mathrm{i}\hbar}[\mathcal{H}(t),\, \rho(t)] + R(t). \tag{6}$$

We use the expressions of Tremblay and Jacques [28] and extend their expressions to include the effects of two counter-propagating beams. Because both of our frequencies come from one laser, then are frequency shifted by an independent RF source into two frequencies, we assume as in [25] that the contribution of the laser linewidth to the ground-state relaxation rate vanishes. We observed short timescale jitter of several hundred Hertz in the RF sources and have, therefore, included a 500 Hz linewidth from RF sources in the ground-state relaxation rate (see [28], equation (2.37)). The external B field is included in Zeeman shifts of the magnetic sublevels. Primarily, we consider an isotropic initial ground-state distribution, but also consider an initial anisotropy as a systematic uncertainty. The calculation was carried out by numerically solving the density matrix equations, i.e., the 128 complex coupled differential equations of the 16-level system of figure 3. Additionally, an arbitrary transverse magnetic field B_x, which can drive transitions with $\Delta F = 0$, $\Delta m_F = \pm 1$, is included using the expressions in [29].

This model includes the two depolarizing mechanisms, discussed in sections 2.2 and 2.3, that lead to $|P| < 1$: ellipticity in the OP light and a transverse magnetic field (B_x) which causes Larmor precession out of the stretched state. Note that since we are pumping both ground state hyperfine levels to prevent losses to the $F = 1$ state, these are the *only* two depolarizing mechanisms. We also consider the false polarization signal potentially produced by coherent population trapping (CPT) states in section 4.

The transverse magnetic field and s_3 are highly correlated when observing the photoionization rate: both lead to a larger fraction of unpolarized atoms and an increase in the photoionization rate. When this model is fit to the experimental data as described in section 5.1, either of these mechanisms, or any combination of them, can equally well account for the observed steady-state photoionization and are therefore highly correlated (>98%). However, the unpolarized population is distributed differently among the $|m_F| < F$ sublevels depending on the relative importance of the light ellipticity and the transverse magnetic field in driving atoms out of the stretched state. Since the unpolarized atoms make a significant contribution to the average nuclear polarization, the relative significance of these two depolarizing mechanisms must be considered.

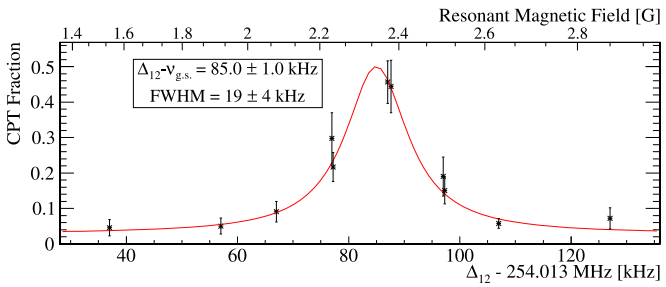

Figure 7. The difference between the two OP frequencies, Δ_{12}, is scanned near the ground state hyperfine resonance of ^{41}K. The resonant frequency is 85 kHz from the ground-state hyperfine splitting, providing a clean measurement of the aligned ($\hat{z}$) magnetic field. The width of this resonance is only 19 kHz and, along with the $m_F = \pm 1$ resonances, is carefully avoided during the ^{37}K experiment.

In order to correctly interpret the photoionization signal as a probe of the total $P_{1/2}$ population, we must consider the relative photoionization cross-sections of the magnetic sublevels. Photoionization from the $P_{1/2}$ state populates outgoing *s*- and *d*-wave photoelectrons with the cross-section proportional to the square of radial ($\mathcal{R}$) and angular portions of the matrix element connecting a pair of final and initial states. Since the angular part does not depend on the details of the central potential, it is well known. Using a single-electron model with a parametric central potential, Aymar, Luc-Koenig, and Combet Farnoux calculate the total cross-section for *s*- and *d*- wave photoelectrons and their results are $\mathcal{R}_d/\mathcal{R}_s \approx 1.7$ at $E_{e^-} = 760$ meV [30].

Considering the off-axis propagation as well as the multiple passes of the UV light (see section 2.4), the total photoionization cross-section changes by no more than 4% in our setup compared to the assumption that all states have an equal probability to be photoionized. The polarization results change by $<10^{-5}$ assuming a 50% uncertainty on the ratio $\mathcal{R}_d/\mathcal{R}_s$.

4. Coherent population trapping

The multi-level system of figure 3 can support CPT states on three distinct sets of λ-atomic systems ($m_F = -1,\ 0,\ 1$). These states are especially problematic for this measurement as atoms in these states are not available to be photoionized and detected, exactly mimicking our experimental signature for good polarization, while simultaneously having $|P| < 1$. Although CPT states are adequately described by the model of section 3, we describe both how their formation is eliminated in our setup as well as the steps that we have taken to verify this.

First, the OP light is retroreflected such that it interacts with the atomic cloud twice: first propagating along $+\hat{z}$ and second along $-\hat{z}$. Since these relative velocities are different for the two passes, the relative Doppler shift of the light frequency between the first and second pass greatly reduces the CPT effect in all but the coldest atoms.

To verify that they are destroyed, we performed measurements with ^{41}K. We measure the magnitude of the CPT state similarly to [25] by optically pumping the atoms with Δ_{12} set to intentionally create CPT states (see figure 3). After the atoms are optically pumped, we switch the frequency of the $F = 1 \rightarrow F' = 2$ laser away from this resonance, destroying the CPT state and allowing the atoms that had been trapped in this state to be optically pumped to the $m_F = \pm F$ state, creating a second burst of photoionization. The relative size of the two photoionization bursts is a measurement of the CPT fraction.

We scan the OP frequency around the $m_F = 0$ ground-state hyperfine resonance as shown in figure 7 and observe that the CPT resonance in our system has a FWHM of only 19 $\pm$ 4 kHz. We avoid this narrow resonance, as well as the $m_F = \pm 1$ resonances, during the polarization measurement by setting Δ_{12} to be 1.1 MHz from the ground-state hyperfine splitting. Simultaneously, since the resonant CPT frequency is equal to the energy difference between the two $m_F = 0$ ground states, we use this to determine the aligned magnetic field from the second-order Zeeman shift: $B_z = 2.339(10)$ G.

5. Results

5.1. Photoionization fits

Figure 8 shows a typical photoionization curve recorded during the experiment. The MOT magnetic field and lasers are switched off at $t = 0$. There was no MOT or OP light interacting with the atoms until the OP light was

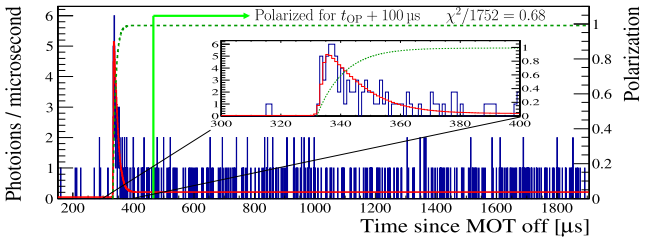

Figure 8. Result of the fit to the σ^- polarization state with $t_{OP} = 332$ μs and $E = 535$ V cm^{-1}. The data is shown as the blue histogram and overlaid with the fit result in red. The nuclear polarization is shown in dark green and quickly approaches one as atoms accumulate in the stretched state.

turned on at $t = t_{OP} = 332$ μs. This was done in order for the MOT magnetic field to die away as it would spoil the final polarization as well as to give a long enough light-free region that we use to measure backgrounds.

The atoms are fully polarized after 100 μs and are re-trapped by the MOT at $t = 1906$ μs after expansion from 2.0 to 4.5 mm FWHM. Separate photoionization curves were recorded for the two polarization states. This histogram is fit to the OP calculation, and the best-fit values are used to calculate the nuclear polarization and alignment according to equations (2) and (3).

We include a constant background rate in the fitting function. In order to separate this background from the residual photoionization that results from unpolarized atoms, we extend the fitting region to begin at $t = 150$ μs, before the OP has begun. At this point, there is no light, either from the MOT or the OP light, illuminating the atoms. Therefore, all events between this point and t_{OP}, when the OP is turned on, are considered background. The primary source of background events are random coincidences between the UV pulse and the β-decay of a ^{37}K atom, delayed by the photoion time-of-flight.

Also at this point, the MOT magnetic field has mostly decayed away while still leaving enough time before the OP light is turned on to achieve a good statistical sensitivity on the background level. We also observed a defect in the event timing system which caused the recorded time to be distributed around the actual event time with a width of 1.0 μs and include this in the fit.

The variable fitting parameters were a constant background rate described above, which is parameterized by the average S/N and the OP laser intensity in each polarization state ($\mathcal{I}^{\pm}$). Additionally, the constant transverse magnetic field (B_x) and one parameter describing the laser frequencies were used as free fitting parameters. Of these, the nuclear polarization depends strongly only on B_x. The light ellipticity also strongly influences P, but this is not a free fitting parameter; it is fixed to the values of s_3^{out} shown in table 1. Although the transverse magnetic field is minimized in the experiment by a pair of orthogonal magnetic field coils, its absolute value at the atoms' position has a complicated dependence on eddy currents in the vacuum chamber and is difficult to determine reliably. Therefore, it is best fit directly to the experimental data as is done here.

Other parameters, including the laser frequencies, were held constant during the fit. Note that both $\Delta(\sigma^-) - \Delta(\sigma^+) = 4.0$ MHz and $\Delta_{12} = 239.2$ MHz are well defined experimentally and the laser linewidth is 0.2 MHz. Therefore, only one overall parameter is required to describe the laser frequencies. We determine this overall frequency by fixing the laser intensity in the two polarization states such that $\mathcal{I}^+ = \mathcal{I}^-$ and fitting the photoionization data to obtain the best-fit value of $\Delta(\sigma^-) = -2.8 \pm 0.2$ MHz, which is consistent with the direct resonance measurement [19, 31]. Finally, the magnetic field (B_z) is taken from the CPT resonance measurement described in section 4.

Throughout the data collection, we varied the time at which we turned on the OP light ($t_{OP} = 332, 432, 732$ μs) as well as the strength of the uniform electric field to collect photoions (395, 415, 535 V cm^{-1}). This resulted in five distinct datasets (not every combination was used). Each dataset was independently fit with the binned maximum likelihood method, this time *not* requiring that $\mathcal{I}^+ = \mathcal{I}^-$, and the results for the nuclear polarization calculated using the best-fit parameters are shown in figure 9. The differences in statistical sensitivity are a result of spending different amounts of time collecting data at the various conditions. Since there is no significant difference among datasets, we conclude that the polarization remained constant throughout the roughly two weeks of data taking.

Taking this into account, we performed the final analysis by fitting each dataset simultaneously to one set of OP parameters. Since the gain of the recoil MCP detector fluctuated throughout the run, each set was fit with an independent S/N representing a constant background in the detector for a total of eight free fitting parameters ($\mathcal{I}^{\pm}$, B_x, and $(S/N)_{A-E}$). The results are shown graphically in figure 10 and summarized in table 2.

The photoion spectra of figure 10 indicate a slight decrease in the partially polarized population even after the atoms are considered fully polarized. This is a result of the AC-MOT quadrupole field, and the eddy currents

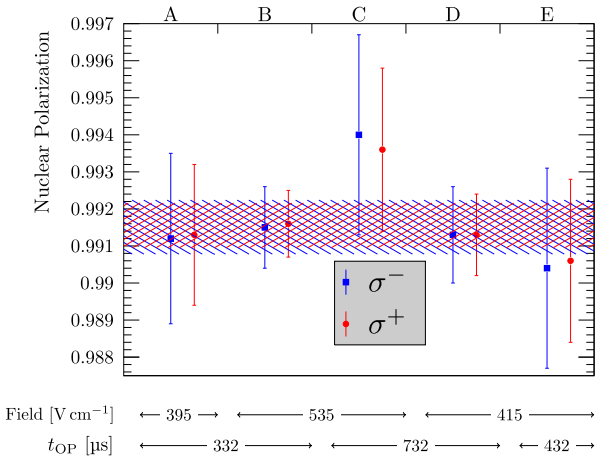

Figure 9. The polarization we find as a result of fitting each set of data independently. The cross-hatched region shows the 1σ uncertainty on the polarization when combining the results of fitting each dataset this way. Note that the two polarization states are not independent as the transverse magnetic field is the same in both cases. Since there is no difference between sets, the final result is fit to all datasets simultaneously.

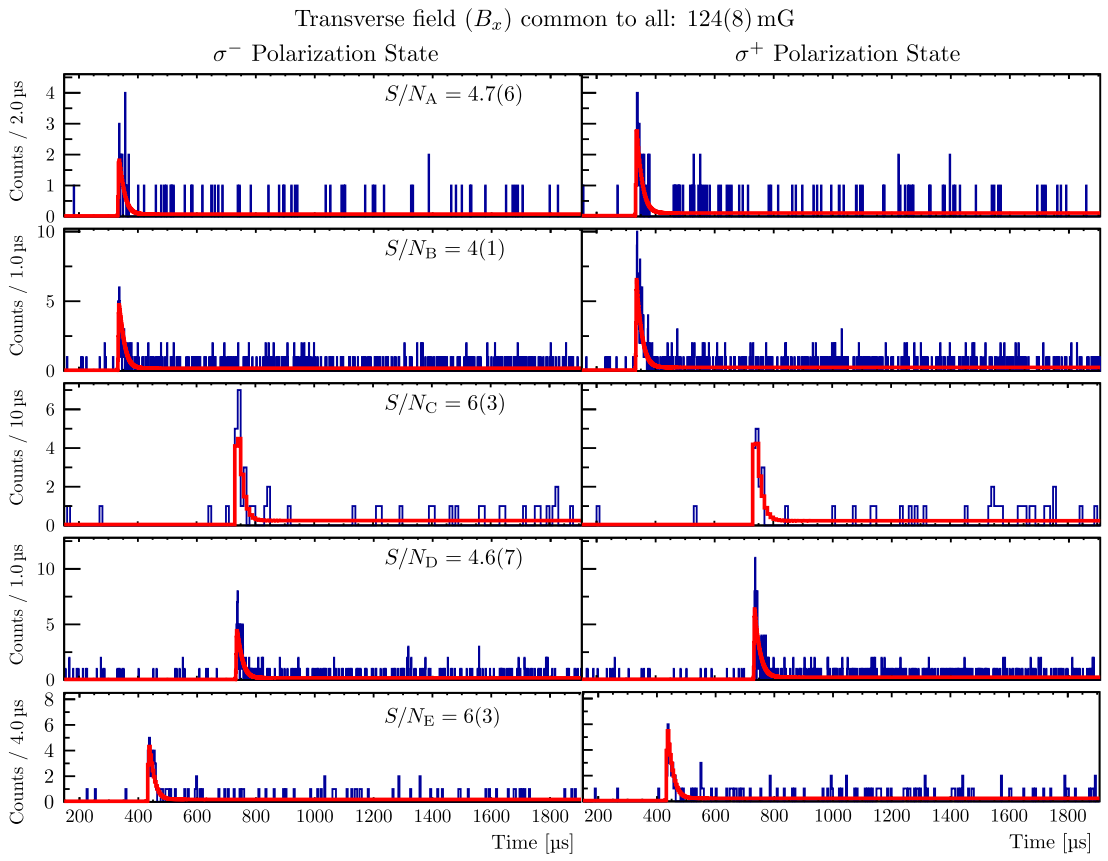

Figure 10. Global fit result including a consistent set of parameters. The Stokes parameter, s_3, was fixed at its experimentally determined value. A single transverse magnetic field, B_x, and separate laser intensities for each polarization state were fit to the entire dataset. The signal-to-noise ratios (S/N_{A-E}) were allowed to vary independently for each of the five datasets. Other parameters were fixed as indicated in the text. The binning for each dataset was chosen to be as fine as possible while producing roughly equal peak bin contents in each set. The effects of using a uniform binning are discussed in section 5.2. The datasets shown here from top to bottom correspond to the conditions shown in figure 9 from left to right.

it creates, slowly decreasing with time. The polarization results dividing the time when the atoms are fully polarized into quadrants are shown in figure 11. All of the data collected with $t_{OP} = 332$ μs is shown as this has the most sensitivity to this effect. This figure indicates that the polarization is improving even after 100 μs of OP,

Table 2. Results from the global polarization fit shown in figure 10.The uncertainties listed here are purely statistical; the result of propagating the systematic uncertainties are discussed in the text.

Parameter	σ^-	σ^+
Misaligned field, B_x (mG)	124(8)	
Average S/N	4.7(6)	
Laser intensity (W m^{-2})	2.33(19)	2.26(13)
Nuclear polarization	−0.9912(7)	+0.9913(6)
Nuclear alignment	−0.9761(21)	+0.9770(17)

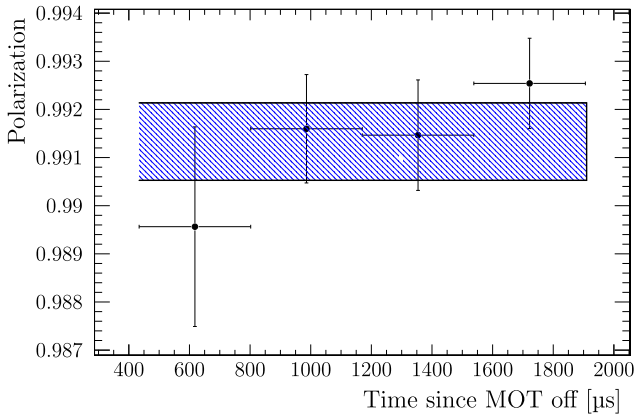

Figure 11. Time dependence of the nuclear polarization in the σ^+ state. The shaded region shows the result with all the data considered while each point considers only the data in the indicated range in addition to the initial OP peak. The polarization seems to improve slightly with time, indicating a gradual decrease in B_x.

although the magnitude of this effect is only $\sim 1\sigma$. Keeping this in mind, we reiterate that the results shown throughout this article represent the average polarization from $t_{\mathrm{OP}} + 100\ \mu\mathrm{s} \rightarrow 1906\ \mu\mathrm{s}$.

5.2. Systematic uncertainties

In this section, we discuss the systematic uncertainties in the fitting routine and lay out the procedure we used to quantify them.

The final results are determined by performing a global fit to all datasets at once. However, it is also possible to find the weighted average of results in figure 9 where each dataset is fit independently. The difference between these two analysis choices gives a systematic uncertainty of 2×10^{-4}. Note that if we fit each dataset independently, there are a total of twenty fitting parameters: $\mathcal{I}^{\pm}$, B_x, and a (S/N) for each of the five datasets. Therefore, the global fit is preferred simply because it captures the same physics with fewer fitting parameters.

The uncertainty on the s_3 parameter is propagated to the final result by varying the input s_3^{out} value by $\pm 1\sigma$ and comparing the results. Although we do not expect the light's polarization to be correlated in the two polarization states, we conservatively treat them as though they are. This procedure gives the most variation in the relative strengths of the two depolarizing mechanisms, resulting in the largest difference in average nuclear polarization. Even with this conservative approach, the systematic uncertainty is at most 2×10^{-4} and does not limit the measurement.

Next, the dependence of the results on the binning of the data is studied by fitting the data with bins of width 1, 2, 5, 10, 20 μs. The central value is taken from the fit with varying bin widths shown in figure 10 and we take the largest difference between any choice of binning and this value as the systematic uncertainty.

As described in section 5.1, we determine one overall frequency by fitting the photoionization data with the requirement that $\mathcal{I}^+ = \mathcal{I}^-$. Since this requirement is only approximately true, we relax this requirement when determining the final results. However, we conservatively treat this condition as a systematic uncertainty. We measure the cloud's overall sail velocity as well as its temperature by comparing the position and size of the photoion spectrum before and after OP. The atoms are moving with an overall sail velocity of 0.05 mm ms^{-1}, which produces a negligible Doppler shift of 69 kHz. We measure a temperature of 2.84 mK, producing a Doppler shift at the rms velocity of 1.0 MHz. Our method of fitting Δ to the photoionization data accounts for

Table 3. Uncertainty budget for the nuclear polarization and alignment measurements. The largest systematic uncertainty arises from the potentially non-zero initial alignment (T_0) of the atoms, which we modeled as described in the text. Also significant is the choice to perform a global fit rather than average the result of each dataset after a series of individual fits. The choice to prefer the global fit is justified by considering the lower number of fit parameters using this method.

Source	ΔP [$\times 10^{-4}$]		ΔT [$\times 10^{-4}$]	
	σ^-	σ^+	σ^-	σ^+
Systematics				
Initial alignment	3	3	10	8
Global fit versus average	2	2	7	6
Uncertainty on s_3^{out}	1	2	11	5
Cloud temperature	2	0.5	3	2
Binning	1	1	4	3
Uncertainty in B_z	0.5	3	2	7
Initial polarization	0.1	0.1	0.4	0.4
Require $\mathcal{I}_+ = \mathcal{I}_-$	0.1	0.1	0.1	0.2
Total systematic	5	5	17	14
Statistics	7	6	21	17
Total uncertainty	9	8	27	22

the sail velocity, and we have calculated the effect of a finite temperature using a rate equation model with a measured 9% difference in the intensity of the two OP beams. We include the difference from the zero temperature case as a systematic uncertainty and find that the uncertainty is larger in the σ^- case, 2.3×10^{-4}, than in the σ^+ case, 0.5×10^{-4}. We attribute this difference to the asymmetry introduced by the aligned magnetic field.

The magnetic field (B_z) has been measured by two independent methods: the Hall probe technique described in section 2.3 and the CPT field measurement described in section 4. Because the Hall probe measurement was performed in air with one vacuum flange removed and without the presence of the electrostatic hoops or MCP assembly, it is expected to be less reliable than the CPT measurement. The results of these two measurements differ by 180 ± 20 mG, which is significantly larger than the uncertainty of the CPT measurement itself. Conservatively, this difference is treated as a systematic uncertainty rather than propagating the smaller uncertainty on the CPT measurement.

Finally, we allow a possible anisotropy in the initial ground-state sublevel distribution of the atoms and characterize this by an initial polarization P_0 and alignment T_0. We measure P_0 by observing the β-asymmetry of the positrons emitted in the ^{37}K decay before the OP light is turned on. Comparing this to the expected asymmetry ($A_\beta = -0.5706$), we conservatively measure an initial polarization $|P_0| < 0.022$. Including an initial population distribution with this distribution produces a systematic uncertainty of 1×10^{-5}.

However, T_0 does not produce a signal in the nuclear decay that we can measure with the current setup. In order to constrain this possibility, we model the sublevel distribution of the MOT on the D_2 ($F = 2 \rightarrow F' = 3$) transition. The vertically ($\hat{z}$) propagating beams combine to produce a linearly polarized standing wave in the x–y plane, while the orthogonal arms produce linearly polarized standing waves in the x–z and y–z planes, which represent a combination of linearly and circularly polarized light along the $\hat{z}$ quantization axis. Since the atom velocities are Doppler limited, their motion averages over the polarization gradients of the resultant electric field. Each pair of $\sigma^\pm$ beams have equal power and the ratio of total power propagating along x:y:z is 2:2:1 so that the effective ratio of linearly to circularly polarized light is 3:2. Since the AC-MOT is deliberately turned off with B_z^{MOT} close to zero, we adopt the value of $B_z^{\text{MOT}} = 100$ mG. Since a transverse magnetic field would only serve to decrease the anisotropy, we assume that it is zero for this calculation. The resulting population distribution has $T_0 = 0.03$. Adopting a conservative uncertainty, we constrain the maximum initial alignment to $T_0 < 0.06$ and compare the results. These systematic uncertainties are summarized in table 3.

At the current level of precision, the total systematic uncertainty is of similar, but slightly smaller, magnitude as the statistical uncertainty. Since the model that is fit to the experimental data only needs to account for the small contribution to the average polarization from the unpolarized population, all of the uncertainties as well as the statistical uncertainty can be reduced by improving both the light polarization and further minimizing the transverse magnetic field to reduce the unpolarized population that must be modeled. The final results are:

$$P(\sigma^+) = +\,0.9913(8) \qquad T(\sigma^+) = -0.9770(22),$$
$$P(\sigma^-) = -\,0.9912(9) \qquad T(\sigma^-) = -0.9761(27) \tag{7}$$

which represent an order of magnitude improvement compared to previous work [11, 14].

6. Discussion

This nuclear polarization measurement is more precise than previous measurements with the same technique and will not dominate the final uncertainty on A_β compared to the statistical uncertainty of $\Delta A_{\rm obs}/A_{\rm obs} = 0.2\%$. We note that the current polarization measurement is limited primarily by statistics: the total systematic uncertainty is only 5×10^{-4}. Therefore, we conclude that future measurements can be sensitive enough to allow correlation parameter measurements at the 0.1% level without significant changes to the techniques described here. In addition, modest improvements to the apparatus will allow for an even-more-precise measurement of the polarization in future experiments.

In the work of a separate group at Los Alamos National Laboratory, samples of $\sim 10^5$ stable ^{85}Rb atoms were polarized to 99.2% $\pm$ 0.2% in a far-off-resonance dipole force trap [32]. Polarization determination was in the same atom cloud location and using similar number of atoms as a planned ^{82}Rb β-decay experiment. The polarization determination combined microwave excitation, a resonant laser push beam, and subsequent retrapping to select Zeeman substates. This determination changed the polarization of the atom cloud, but was done with high precision in short times, allowing probing of representative samples of atoms.

Further increasing the light polarization and decreasing the transverse magnetic field will both increase the average polarization and decrease its uncertainty. With less unpolarized population to model, the uncertainty about its distribution will lead to less uncertainty on the nuclear polarization and alignment. Therefore, we emphasize that improving the polarization will simultaneously improve the precision that we can reach. Although we are continuing to optimize the light polarization ($s_3^{\rm out}$), some optical elements, particularly the liquid crystal variable retarder, preserve the polarization better in one state than the other making it difficult to optimize both polarization states simultaneously. Improvements to the trim coil system used to reduce the transverse magnetic field can also reduce the polarization uncertainty. For example, if the magnetic field is reduced to 1/2 its current value and no other parameters are changed, the statistical uncertainty is reduced by the same factor. With careful measurements using ^{41}K, we expect to be able to achieve this improvement. In particular, there is enough information from ^{41}K atoms to trim the gradient of the magnetic field on each axis in addition to zeroing the average value. Since we expect the systematic uncertainties to scale similarly, it seems possible to achieve a polarization uncertainty of $\sim$0.04% in upcoming measurements, allowing for an uncertainty of $\sim$0.1% on the polarized correlation parameters.

7. Conclusions

In this paper, we have reported a precise *in situ* measurement of the nuclear polarization and alignment in optically pumped ^{37}K. The same dataset used in these measurements contains enough β-decay data to make a measurement of the β-asymmetry (A_β) with an expected relative uncertainty of $<0.5\%$. We will report these results in a future publication. Furthermore, this work has demonstrated the capability to measure the nuclear polarization to $<10^{-3}$, which motivates future development towards measurements of polarized β-decay correlations at this level of precision.

Acknowledgments

We gratefully acknowledge the support staff of TRIUMF and ISAC and thank S Gensemer and A Hatakeyama for alerting us to the effects of CPT in optical pumping as well as J Zhang for help with weld permeability measurements. This work was supported by the U S Department of Energy under Grant No. DE-FG02-11ER41747 and DE-FG02-93ER40773, by the Natural Sciences and Engineering Research Council of Canada, and by the Israel Science Foundation. TRIUMF receives federal funding via a contribution agreement with the National Research Council of Canada.

References

[1] Holstein B R and Treiman S B 1977 Tests of spontaneous left–right-symmetry breaking *Phys. Rev.* D **16** 2369–72
[2] Naviliat-Cuncic O, Girard T A, Deutsch J and Severijns N 1991 Left–right symmetry breaking sensitivity of beta -asymmetry measurements *J. Phys. G: Nucl. Part. Phys.* **17** 919
[3] Herczeg P 2001 Beta decay beyond the standard model *Prog. Part. Nucl. Phys.* **46** 413–57

[4] Severijns N, Beck M and Naviliat-Cuncic O 2006 Tests of the standard electroweak model in nuclear beta decay *Rev. Mod. Phys.* **78** 991–1040
[5] Severijns N, Tandecki M, Phalet T and Towner I S 2008 $\mathcal{F}t$ values of the $T = 1/2$ mirror β transitions *Phys. Rev.* C **78** 055501
[6] Naviliat-Cuncic O and Severijns N 2009 Test of the conserved vector current hypothesis in $T = 1/2$ mirror transitions and new determination of $|V_{ud}|$ *Phys. Rev. Lett.* **102** 142302
[7] Hardy J C and Towner I S 2015 Superallowed $0^+ \rightarrow 0^+$ nuclear β decays: 2014 critical survey, with precise results for V_{ud} and CKM unitarity *Phys. Rev.* C **91** 025501
[8] Cirigliano V, Gardner S and Holstein B R 2013 Beta decays and non-standard interactions in the {LHC} era *Prog. Part. Nucl. Phys.* **71** 93–118
[9] Harvey M and Murray A J 2008 Cold atom trap with zero residual magnetic field: the ac magneto-optical trap *Phys. Rev. Lett.* **101** 173201
[10] Anholm M 2011 Characterizing the AC-MOT *MSc* The University of British Columbia
[11] Melconian D *et al* 2007 Measurement of the neutrino asymmetry in the decay of laser-cooled, polarized ^{37}K *Phys. Lett.* B **649** 370–5
[12] Melconian D G 2005 Measurement of the neutrino asymmetry in the βdecay of laser-cooled, polarized ^{37}K *Doctoral* Simon Fraser University
[13] Jackson J D, Treiman S B and Wyld H W 1957 Possible tests of time reversal invariance in beta decay *Phys. Rev.* **106** 517–21
[14] Behling R S 2015 Measurement of the standard model beta asymmetry parameter, A_β in ^{37}K *Doctoral* Texas A&M University
[15] Gay T J and Dunning F B 1992 Mott electron polarimetry *Rev. Sci. Instrum.* **63** 1635–51
[16] Plaster B *et al* 2012 Measurement of the neutron β-asymmetry parameter A_0 with ultracold neutrons *Phys. Rev.* C **86** 055501
[17] Behr J A and Gorelov A 2014 -decay angular correlations with neutral atom traps *J. Phys. G: Nucl. Part. Phys.* **41** 114005
[18] Melconian D *et al* 2005 Release of K from catcher foils *Nucl. Instrum. Methods Phys. Res.* A **538** 93–9
[19] Behr J A *et al* 1997 Magneto-optic trapping of β-decaying ^{38}K^m, ^{37}K from an on-line isotope separator *Phys. Rev. Lett.* **79** 375–8
[20] Swanson T B, Asgeirsson D, Behr J A, Gorelov A and Melconian D 1998 Efficient transfer in a double magneto-optical trap system *J. Opt. Soc. Am.* B **15** 2641–5
[21] Wang B, Han Y, Xiao J, Yang X, Zhang C, Wang H, Xiao M and Peng K 2007 Preparation and determination of spin-polarized states in multi-Zeeman-sublevel atoms *Phys. Rev.* A **75** 051801
[22] Smith G A, Silberfarb A, Deutsch I H and Jessen P S 2006 Efficient quantum-state estimation by continuous weak measurement and dynamical control *Phys. Rev. Lett.* **97** 180403
[23] Julsgaard B, Sherson J, Sørensen J L and Polzik E S 2004 Characterizing the spin state of an atomic ensemble using the magneto-optical resonance method *J. Opt. B: Quantum Semiclass. Opt.* **6** 5
[24] Kobayashi S, Yamamoto Y, Ito M and Kimura T 1982 Direct frequency modulation in AIGaAs semiconductor lasers *IEEE J. Quantum Electron.* **18** 582–95
[25] Gu S, Behr J, Groves M and Dhat D 2003 Coherent population trapping states with cold atoms in a magnetic field *Opt. Commun.* **220** 365–70
[26] Tanaka U and Yabuzaki T 1993 Simultaneous improvement of short- and long-term frequency stability of a diode laser *Proc. SPIE* **1837** 70–80
[27] Warner C L, Behr J A and Gorelov A 2014 PCTFE as a solution to birefringence in atom trap viewports *Rev. Sci. Instrum.* **85** 113106
[28] Tremblay P and Jacques C 1990 Optical pumping with two finite linewidth lasers *Phys. Rev.* A **41** 4989–99
[29] Renzoni F, Cartaleva S, Alzetta G and Arimondo E 2001 Enhanced absorption Hanle effect in the configuration of crossed laser beam and magnetic field *Phys. Rev.* A **63** 065401
[30] Aymar M, Luc-Koenig E and Farnoux F C 1976 Theoretical investigation on photoionization from Rydberg states of lithium, sodium and potassium *J. Phys. B: At. Mol. Phys.* **9** 1279
[31] Rossi D M *et al* 2015 Charge radii of neutron-deficient ^{36}K and ^{37}K *Phys. Rev.* C **92** 014305
[32] Fang F, Vieira D J and Zhao X 2011 Precision polarization measurements of atoms in a far-off-resonance optical dipole trap *Phys. Rev.* A **83** 013416